A set of molecular models for alkaline-earth cations in aqueous solution

Stephan Deublein,[†] Steffen Reiser,[†] Jadran Vrabec,[‡] and Hans Hasse[*,†]

Lehrstuhl für Thermodynamik, Technische Universität Kaiserslautern, 67653 Kaiserslautern, Germany, and Lehrstuhl für Thermodynamik und Energietechnik, Universität Paderborn, 33098 Paderborn, Germany

E-mail: hans.hasse@mv.uni-kl.de

---

[*]To whom correspondence should be addressed
[†]Lehrstuhl für Thermodynamik, Technische Universität Kaiserslautern, 67653 Kaiserslautern, Germany
[‡]Lehrstuhl für Thermodynamik und Energietechnik, Universität Paderborn, 33098 Paderborn, Germany

Abstract

New Lennard-Jones plus point charge models are developed for alkaline-earth cations. The cation parameters are adjusted to the reduced liquid solution density of aqueous alkaline-earth halide salt solutions at a temperature of 293.15 K and a pressure of 1 bar. This strategy is analogous to the one that was recently used for developing models for alkali and halide ions so that both model families are compatible. The force fields yield the reduced liquid solution density of aqueous alkaline-earth halide solutions in good agreement with experimental data over a wide range of salinity. Structural microscopic properties, i.e. radial distribution function and hydration number, are predicted in a good agreement with experimental and quantum chemical data. The same holds for dynamic properties, namely hydration dynamics, self-diffusion coefficient and electric conductivity. Finally, the enthalpy of hydration of the salts in aqueous solution was favourably assessed.

1. Introduction

Aqueous electrolyte solutions play an important role in many natural processes and industrial applications. Their thermodynamic properties are dominated by the strong electrostatic interactions between the ions and the solvent molecules. In technical applications, however, not only the charges and ionic strengths are relevant, but the individual nature of the different ions is important as well. Thus most electrolyte solutions are outside of the regime which can be described with the approach by Debye and Hückel.[1,2] Therefore, different empirical extensions of the Debye-Hückel limiting law have been suggested,[3–7] which consider the non-electrostatic interactions between the ions. These models introduce a large number of adjustable parameters so that they often serve as correlation tools only. Molecular simulations of electrolyte solutions go far beyond these models. They allow for detailed insights into the properties of electrolyte solutions and for predictions of their properties. The prerequisite are accurate molecular force fields. The goal of the present study is the development of such models for alkaline-earth cations.

Force fields for alkaline-earth cations have been developed since the 1980s by different groups and

have been used in various types of studies.[8,9] The most common model type is a Lennard-Jones (LJ) sphere with the unit charge of magnitude $+2e$ in its center. These models, hence, only differ with respect to their LJ parameters. Ion models for magnesium[10] and calcium[11] were developed from ab initio calculations and were evaluated regarding their ability to predict structural properties of solutions. Guardia et al.[12] extended the analysis to the potential of mean force, while Koneshan et al.[13] studied some of the these models with respect to transport properties. Åqvist[14] derived force fields for alkaline-earth cations based on the free energy perturbation theory. These force fields were further improved under the label ff99[15] and are part of the AMBER[16] package. Spangberg et al.[17] developed two different molecular models for magnesium from ab initio calculations: one model explicitly considers three-body interactions, the other one explicitly considers polarization effects. For aqueous $MgCl_2$ solutions, both models describe the first hydration shell around the ions in good agreement with experimental data, while only the three-body model yields a reliable solvation enthalpy of the salt.[17] Jiao et al.[18] developed force fields for magnesium and calcium from ab initio calculations using a polarizable potential. For chloride solutions, these models reproduce the solvation free energy in good agreement with experimental data. For an aqueous $CaCl_2$ solution, the self-diffusion coefficient of the cation was also well predicted, while for the magnesium model, it was significantly underpredicted.[18] Megyes et al.[19] developed a simple LJ based model for calcium in aqueous $CaCl_2$ solutions that yields the structural properties in good agreement with experimental values. Gavryushov et al.[20] published effective ion potentials for all alkaline-earth chloride salts, neglecting the long range contributions of the electrostatic interactions between the ions. These models were used for the calculation of thermodynamic properties, e.g. the activity coefficient,[20] describing the solvent implicitly.

This short literature survey shows that significant effort was spent on the development of force fields for some alkaline-earth cations, however, a comprehensive approach is still lacking.

In the present work, a set of molecular models for all non radioactive alkaline-earth cations, i.e. Be^{2+}, Mg^{2+}, Ca^{2+}, Sr^{2+} and Ba^{2+}, was developed for aqueous solutions. The models follow the classical approach, i.e. they describe the ions by one LJ sphere with one superimposed point

charge with a magnitude of $+2e$. This simple model type is supported by all common molecular simulation codes.[21,22]

The LJ model parameters were adjusted to experimental data on the reduced liquid solution density of aqueous alkaline-earth halide solutions. This approach was used in preceding work for developing a set of molecular models for alkali and halide ions.[23] Throughout the present study, the halide ion models were taken from that work,[23] while water was described by the SPC/E model.[24] However, the results from our previous study[23] suggest that the simulation results for the reduced liquid solution density do not strongly depend on the choice of the water model and hence, the ion models presented here should also be applicable in combination with other water models. Section 2 introduces the parameterization method, while in Section 3, details on the simulations of the studied properties are given. In Section 4, simulation results are shown for the density, structural, dynamic and caloric properties, while Section 5 concludes the work.

2. Force field development

The force field type employed in this study was the standard LJ 12-6 potential plus coulombic interactions

$$u_{ij} = 4\varepsilon_{ij}\left(\left(\frac{\sigma_{ij}}{r_{ij}}\right)^{12} - \left(\frac{\sigma_{ij}}{r_{ij}}\right)^{6}\right) + \sum_{l=1}^{N_{C,i}}\sum_{m=1}^{N_{C,j}}\frac{q_l q_m}{4\pi\varepsilon_0 r_{lm}}, \tag{1}$$

where u_{ij} is the potential energy between the particles i and j with a distance r_{ij} between their LJ sites. σ_{ij} and ε_{ij} are the LJ parameters for size and energy, respectively, q_l and q_m are the charges of the solute or the solvent molecules that are at a distance r_{lm}, and ε_0 is the vacuum permittivity. The indices l and m count the point charges, while the total number of charges of molecule i is denoted by $N_{C,i}$. Note that Eq. (1) is given in a form that includes the interactions with water. Throughout the present simulations, the Lorentz-Berthelot combining rules[25,26] were applied for the unlike LJ interactions. Technical details of the employed simulation methods are given in the Appendix. Note here that the employed simple force field does not capture the physical effects of polarization. This effect, however, is included in the force field by the parameterization strategy

4

that was used for the force field development and which is introduced in detail the last part of this section.

The solvent water was modeled by the rigid, non-polarizable force field SPC/E,[24] which consists of one LJ sphere and three point charges. It is widely used for molecular simulations of biomolecules, often in combination with the GROMOS force field.[27] The SPC/E water model yields a decent agreement with the experimental liquid density of pure water at ambient conditions of $T = 293.15$ K and $p = 1$ bar.[23]

The ions were modeled by one LJ sphere with one point charge of magnitude $+2$ e in their center. The halide anion force fields are of the same type and were taken from preceding work.[23] For the molar mass of all particles, the experimental values were used. For parameterization, the cation LJ size parameter σ_c was adjusted to reproduce the reduced liquid solution density $\widetilde{\rho}$ over salinity x at the temperature $T = 293.15$ K and the pressure $p = 1$ bar. Here, $\widetilde{\rho}$ is defined by the density of the electrolyte solution ρ and the density of the pure solvent water ρ_O at the same temperature T and pressure p

$$\widetilde{\rho} = \frac{\rho}{\rho_O} \; . \tag{2}$$

These data were taken from the literature and were typically measured by vibrating tube densimeter or hydrometer. It was shown recently[23] that the reduced density $\widetilde{\rho}$ depends only very weakly on the LJ energy parameter. Following the same approach here, the cation LJ energy parameter ε_c was set to $\varepsilon_c/k_B = 200$ K for all models. This choice yields reasonable values for the osmotic coefficient of various alkali halide solutions.[28]

The dependence of $\widetilde{\rho}$ on x was approximated by a first order Taylor expansion around the pure water ($x = 0$) state point

$$\widetilde{\rho}(x) = \widetilde{\rho}(x = 0) + \frac{\mathrm{d}\widetilde{\rho}}{\mathrm{d}x}\bigg|_{x=0} x + O^2 = 1 + mx + O^2 \; . \tag{3}$$

The short notation m stands for the derivative of $\widetilde{\rho}$ with respect to the salinity x, i.e. the mass fraction of the salt in solution, at infinite dilution and O^2 contains all higher order terms of the

expansion. The quantity m is well accessible from experimental solution density data by simple derivation. Plots of the these data show an almost linear behavior of $\rho(x)$ up to high salinities, cf. Figure 1. The mass fraction was used in the present work to specify the salinity rather than other common measures like molality or ion strength as the linear range turns out to be particularly large when the mass fraction is used. Other advantages of this force field parameterization with respect to the reference $\widetilde{\rho}$ were discussed in more detail before[23] and are not repeated here.

For the present parameterization, the cation LJ size parameter σ_c was systematically varied between 1.5 and 4.5 Å with increments of 0.5 Å and regressed using a polynomial function. By molecular simulation with varying low salinity, the increase of the reduced density with increasing salinity in aqueous alkaline-earth solutions was determined. The parameter σ_c for the cations was subsequently adjusted to the derivative m of five solutions, namely $BeCl_2$ (the only water soluble beryllium salt), $MgBr_2$, $CaBr_2$, $SrBr_2$ and $BaBr_2$. Fluoride salts were not considered, since they are not soluble in water. Bromide salts were selected for the adjustment, since the employed bromide anion model was found to be very accurate for aqueous alkali bromide solutions.[23] Mathematically, the adjustment leads to a single solution for all five cations. Although the ion force fields only contain experimental information on the five solutions mentioned above, they show good predictive capabilities with respect to other salt combinations containing alkaline-earth cations and halide anions, cf. Section 4. Note that a different parameterization strategy, a global fit of all ion parameters, was also feasible, but was not performed here, cf. Section 4.

3. Structural, dynamic and caloric properties

The electrolyte solutions were analyzed regarding structural properties of the solution, i.e. the radial distribution function (RDF) $g_{i-O}(r)$ of water around the cation i,[29] the hydration number n_{i-O}[30] as well as the potential of mean force w_{i-O}[29] between cation i and water. To study the dynamics in the liquid, the residence time τ_O, the self-diffusion coefficient D_i and the electric conductivity σ of aqueous alkaline-earth solutions were evaluated. In addition, the enthalpy of

hydration for the ions in solution was determined. Throughout these analyses, the position of water molecules was represented by the position of the oxygen site O.

The RDF $g_{i-O}(r)$ of water around the ion i indicates the structure that the ion imposes onto the solution. This quantity is well known from the literature[29] and is not further discussed here. The hydration number n_{i-O} quantifies the number of solvent molecules within a given distance around the ion i. It is defined by

$$n_{i-O} = 4\pi\rho_O \int_0^{r_{\min}} r^2 g_{i-O}(r) \mathrm{d}r \, , \tag{4}$$

where ρ_O is the number density of water and $r_{\min}$ is the distance up to which the hydration number is calculated. To determine the hydration number within the first shell around the ion, the value $r_{\min,1}$ was chosen to be the distance of the first minimum of the RDF.[30]

The residence time τ_O defines the average time span that a water molecule remains within a given distance r_{i-O} around an ion i. It is related to the following autocorrelation function[13]

$$\tau_O = \frac{1}{n_{i-O}} \int_{t=0}^{\infty} \sum_{k=1}^{n_{i-O}} \Theta_k(t)\Theta_k(0) \mathrm{d}t \, , \tag{5}$$

where Θ is the Heavyside step function which yields unity, if a water molecule is paired with an ion, and t is the time. In this study, the residence time of water in the first hydration shell was determined. A water molecule and an ion were considered as paired, when their mutual distance r_{i-O} was lower than the distance of the first RDF minimum, i.e. $r_{i-O} < r_{\min,1}$. Following a proposal by Impey et al.,[31] unpairing was assumed when the separation $r_{i-O} > r_{\min,1}$ lasts more than 2 ps. However, a short-time pairing of two particles with $\tau_O < 2$ ps was fully accounted for in the calculation of τ_O.

The dynamics of water molecules leaving the first hydration shell was also characterized by the rate coefficient k, which is simply the inverse of the residence time $k = 1/\tau_O$.

The potential of mean force w_{i-O} between the ion i and water can be derived from the orientation-

7

ally averaged ion-water RDF by[13,32,33]

$$w_{i-\text{O}}(r) = -k_{\text{B}}T \ln g_{i-\text{O}}(r) , \tag{6}$$

where k_{B} is the Boltzmann constant. The energy difference between the first minimum of the potential of mean force and its first maximum, where the transition state is located, is the energy barrier that a water molecule has to overcome in order to leave the first hydration shell of the ion. Using transition state theory, the maximum rate coefficient k^{T} for water molecules leaving this shell can be determined according to[13,32]

$$k^{\text{T}} = \sqrt{\frac{k_{\text{B}}T}{2\pi\mu}} \frac{\exp(-\beta w_{i-\text{O}}^{\text{eff}}(r^*))}{\int_0^{r^*} \exp(-\beta w_{i-\text{O}}^{\text{eff}}(r))dr} , \tag{7}$$

where $\mu = m_i m_{\text{O}}/(m_i + m_{\text{O}})$ is the reduced mass of the ion-water pair and $w_{i-\text{O}}^{\text{eff}}$ is the effective potential of mean force between ion and solvent. The distance r^* is set to the distance of the first maximum of the potential of mean force, since the hydration dynamics in the first hydration shell around the cation was targeted in this work. The effective potential of mean force is linked to $w_{i-\text{O}}$ by an additional term that accounts for the increase of the potential of mean force with increasing volume, and hence r, according to[13,32]

$$w_{i-\text{O}}^{\text{eff}}(r) = w_{i-\text{O}}(r) - 2k_{\text{B}}T \ln \frac{r}{r^*} . \tag{8}$$

The maximum rate coefficient k^{T} from transition state theory is related to the rate coefficient k by the transmission coefficient κ

$$\kappa = \frac{k}{k^{\text{T}}} . \tag{9}$$

In addition to hydration dynamics, the self-diffusion coefficient of the ions and the electric conductivity of the aqueous solutions were determined via equilibrium molecular dynamics (MD) simulations by means of the Green-Kubo formalism.[34] This formalism offers a direct relationship between transport coefficients and the time integral of the autocorrelation function of the corre-

sponding fluxes within a fluid. Hence, the Green-Kubo expression for the self-diffusion coefficient D_i is based on the individual ion velocity autocorrelation function[34]

$$D_i = \frac{1}{3N_i} \int_0^\infty \langle \boldsymbol{v}_k(t) \cdot \boldsymbol{v}_k(0) \rangle \mathrm{d}t \ , \tag{10}$$

where $\boldsymbol{v}_k(t)$ is the center of mass velocity vector of ion k of species i at some time t. Eq. (10) is an average over all N_i ions.

The electric conductivity σ is related to the time autocorrelation function of the electric current flux $\boldsymbol{j}(t)$ and is given by[35]

$$\sigma = \frac{1}{3Vk_\mathrm{B}T} \int_0^\infty \langle \boldsymbol{j}(t) \cdot \boldsymbol{j}(0) \rangle \mathrm{d}t \ , \tag{11}$$

where V is the volume. The electric current flux is defined by the charge q_k of ion k and its velocity vector $\boldsymbol{v}_k$ according to

$$\boldsymbol{j}(t) = \sum_{k=1}^{N_\mathrm{Ion}} q_k \cdot \boldsymbol{v}_k(t) \ , \tag{12}$$

where N_Ion is the number of ions in solution. Note that all ions in solutions have to be considered, but not the water molecules. For better statistics, σ was sampled over all three independent spatial elements of $\boldsymbol{j}(t)$. The electric current time autocorrelation function may be decomposed into the sum[36]

$$\langle \boldsymbol{j}(t) \cdot \boldsymbol{j}(0) \rangle = Z(t) + \Delta(t) = \sum_{k=1}^{N_\mathrm{Ion}} \langle q_k^2 \cdot \boldsymbol{v}_k(t) \cdot \boldsymbol{v}_k(0) \rangle + \sum_{k=1}^{N_\mathrm{Ion}} \sum_{\substack{n=1 \\ n \neq k}}^{N_\mathrm{Ion}} \langle q_k q_n \cdot \boldsymbol{v}_k(t) \cdot \boldsymbol{v}_n(0) \rangle \ , \tag{13}$$

where $Z(t)$ is an autocorrelation function and $\Delta(t)$ a crosscorrelation function that quantifies the deviations from the ideal Nernst-Einstein behavior.[30,36]

The first term $Z(t)$ describes the mobility of the ions due to their self-diffusion in solution. Mathematically, it is simply the sum of the self-diffusion coefficients of all ion types in solution weighted by their charges. The second term $\Delta(t)$ describes the correlated motion of the ions in solution. Correlated motions of ion pairs of opposite charges in solution lower the electric conductivity

9

($\Delta(t) < 0$), while correlated motions of ion pairs with the same charge enlarge σ ($\Delta(t) > 0$). The magnitude of the electric conductivity is highly dependent on solution salinity x and increases with higher x for low and medium salinities.

In addition, the enthalpy of hydration of the ions Δh_{hyd} was investigated. It is defined as the difference between the enthalpy of the ions dissolved in the aqueous solution at infinite dilution and the enthalpy of the salt in an artificial ideal gas reference state. Using molecular simulation, Δh_{hyd} is derived from the enthalpy H of the aqueous electrolyte solution and the enthalpy H_O of the pure solvent divided by the amount of salt in solution n_S [37]

$$\Delta h_{hyd} = \frac{H - H_O}{n_S} - RT \ ,$$ (14)

where R is the ideal gas constant. The enthalpy of hydration was determined for all alkaline-earth halide salts individually.

4. Results and discussion

Model parameters

The LJ size parameter values of the alkaline-earth cations determined in the present work are presented in Table 1. The order of the LJ size parameter for the cations is consistent with their order in the periodic table of elements, i.e. $Be^{2+} < Mg^{2+} < Ca^{2+} < Sr^{2+} < Ba^{2+}$. Note that the ionic radii of the ions differ slightly from experimentally determined ionic radii reported in the literature.[38] Similar observations were already reported for alkali halide ions as well.

Reduced liquid solution density

The present ion models were parameterized to reduced liquid solution density data of five alkaline-earth halide salts ($BeCl_2$, $MgBr_2$, $CaBr_2$, $SrBr_2$ and $BaBr_2$) at low salinity. This data was thus matched within the experimental accuracy, cf. Figure 1. At higher salinity as well as for all re-

maining eight electrolyte solutions, the present simulation results for $\widetilde{\rho}$ are predictive. Note that neither the alkaline-earth fluoride salts nor the beryllium halide salts are soluble in water, except for BeCl$_2$. For reference, Table 1 also contains the halide anion parameters.[23]

For the alkaline-earth chloride salts in aqueous solution, the reduced liquid solution density is well predicted at low salinity. The deviations to experimental reduced solution density data are less than 1%. For higher salinity, the present force fields underestimate the experimental data.

For the alkaline-earth bromide salts in aqueous solution, the agreement with experimental data[39] is excellent throughout the entire salinity range, cf. Figure 1. This is not surprising for low salinity, since most of the ion parameters were adjusted to this property. However, also at high salinity, where the experimental data shows a significantly nonlinear behavior, the agreement between simulation and experiment is very good.

With respect to the alkaline-earth iodide salts in aqueous solution, similar results were obtained for the reduced liquid solution density. The deviations between the simulation data and experimental values are below 1% over the entire salinity range, cf. Figure 1. Again, this has to be seen in the light of the fact that the alkaline-earth iodide salts show a nonlinear increase of the solution density with increasing salinity, which the present force fields are able to predict. Note that the good agreement for the aqueous alkaline-earth bromide and iodide solutions are due to the parameterization strategy of only using alkaline-earth bromide salts for the parameter adjustment. A global fit of the model parameters to all alkaline-earth halide salts was possible and would have yielded better results for alkaline-earth chloride salts. However, this improvement for these salts results in significantly higher deviations for the remaining salts. Since the deviations of the alkaline-earth chloride salts could not solely be mapped to the cation model parameters, that global parameterization strategy was not followed.

Hydration properties

After parameterization, all aqueous alkaline-earth solutions were analyzed regarding structural and dynamic solution properties. The investigated structural data are the RDF $g_{i-\text{O}}(r)$[29] of wa-

ter around the ion i and the hydration number n_{i-O}.[30] In addition, the potential of mean force $w_{i-O}(r)$[32] between cation i and water was determined. Furthermore, an analysis with respect to the net charge Q_i around the cations was performed. However, these results contain little information, since for all cations, the net charge had not decayed to a constant value within the cubic simulation volume with an edge length of ≈ 13 Å that were used in the present study. Although charge compensation within the boundaries of the simulation volume is desirable, the simulation error induced by this mismatch should not be important given that periodic boundary conditions were employed.

The analysis of the dynamic properties covered the hydration dynamics of the first hydration shell, i.e. the residence time τ_O during which a water molecule remains within the first hydration shell, as well as the rate and transmission coefficients k, k^T and κ, respectively, which characterize the dynamics of water molecules leaving the first hydration shell. Throughout, the water molecules were represented by their oxygen atom O.

The general trends are individually discussed for each alkaline-earth ion in the following, while the results are summarized in Table 2 and Table 3. For all investigated alkaline-earth cations, the studied properties hardly change with the type of counterion in solution and salinity. E.g., for the cation-water RDF, the positions of the first four extrema, i.e. the two maxima and minima, were found to be constant, which is in good agreement with experimental data.[40,41] A typical RDF of water around the cation Mg^{2+} in an aqueous $MgCl_2$ solution is shown in Figure 2 for two salinities. The first maximum of the RDF is located close to the ion. The peak is very high, reaching up to 20, which is roughly a factor of 2.5 higher than the maximum values observed for alkali cations of approximately the same size.[23] The width of the first peak of the alkaline-earth RDF is small, being in the order of 0.3 Å for small alkaline-earth ions and 0.6 Å for larger ones starting with Ca^{2+}. This is roughly half as wide than in case of monovalent cations.[23] This indicates a highly ordered structure around the cation that is caused by the electrostatic interactions between the cation and the solvent. Due to the cation charge attraction, all water molecules in the first hydration shell are located in the closest vicinity around the cation that is sterically possible. As expected, the

solvent molecules in the first hydration shell are oriented such that the negatively charged oxygen atom is directed towards the cation. This causes the very high peak of the RDF. The small width of the first peak of the RDF can be explained by hindered solvent molecule motions. The electrostatic attraction inhibits not only translational motions of water molecules in form of leaving the first hydration shell, but also constrains the rotational motions of the solvent molecules. The first peak of the RDF is followed by a broad minimum, where $g_{i-O}(r)$ is almost zero. The width of the minimum corresponds to the width of the first hydration shell, where the water molecules are constrained in their motions and solvent molecules from the bulk can hardly penetrate into. For all alkaline-earth cations, a second hydration shell was observed which is also quite pronounced, cf. Figure 2. The peak of the second shell in the RDF reaches a value of 2 for $MgCl_2$ and is slightly lower for larger cations. After the second peak, the RDF decays rapidly to unity, showing almost no indication for the formation of a third hydration shell. The anion-water RDFs were found to be the same as reported for alkali halide solutions in preceding work.[23]

Beryllium: The RDF of beryllium in aqueous $BeCl_2$ solutions exhibits the first maximum at a distance of 2.0 Å and the first minimum at 2.3 Å. These values are both by 0.3 Å larger than experimental data for the first maximum from x-ray diffraction[41] and ab initio calculations performed without counterions,[42] indicating that the molecular model's attractive forces between ion and solvent are too weak. The second maximum of the RDF was found at a distance of 4.2 Å, the second minimum at 4.9 Å. These results differ again from ab initio calculations by 0.4 Å.[42] The hydration number for beryllium in the first shell was determined to be 5-6, which is higher than the experimental number of 4 water molecules around Be^{2+}.[41] The residence time exceeds the total simulation time of 3 ns that was used in the present work, which is in agreement with earlier MD studies.[43] This high residence time in the proximity of the Be^{2+} ion is due to the very strong electrostatic attraction between this cation and the solvent. The energy barrier that a water molecule needs to overcome for leaving the first hydration shell could not be determined explicitly due to the lack of trajectories that show leaving water molecules. These results indicate that the structure around the beryllium cation is very static. Structural disorder only occurs in the second

hydration shell and in the bulk solvent.

Magnesium: For magnesium cations, the first maximum of the RDF was determined at a distance of 2.0 Å, the first minimum at 2.3 Å. This is in agreement with experimental data from x-ray diffraction, which indicate an average ion-water distance of 2.1 Å,[41,44] as well as in agreement with ab initio calculations performed without counterions, which determined the distance to be 2.1 Å as well.[45] The maximum of the second shell was found to be at a distance of 4.2 Å from the ion, the second minimum at 4.9 Å. The first shell hydration number was almost constant at a value of 5.3 to 5.9 water molecules around the cation, independent on counterion type and salinity. Experimentally, a hydration number of 6 was observed.[40,46] Regarding the dynamics of the system, the behavior is similar to the Be^{2+} cation. The water residence time could not be determined for Mg^{2+} within the total simulation time of 3 ns, which is again caused by the strong electrostatic attraction between cation and water molecules. Therefore, the results for the maximum rate constant for a water molecule leaving the first hydration shell from transition state theory k^T could not be determined. The energy barrier associated with a water molecule leaving the first hydration shell was found to be >8 $k_B T$.

Calcium: For the calcium cation, the first maximum and the first minimum of the RDF are shifted to larger distances due to the larger size of Ca^{2+}, being 2.4 and 3.0 Å, respectively. This is in agreement with experimental data, which locate the first maximum at 2.4 Å,[41] and ab initio calculations performed without counterions, which determined the distance to be 2.5 Å.[47] The second extrema of the RDF are located at distances of 4.6 and 5.4 Å, respectively, which match the ab initio distance of 4.6 Å for the second maximum perfectly.[47] The increase of the RDF peak width, especially of the first one, indicates that the water structure around Ca^{2+} is less ordered than in the case of smaller alkaline-earth ions. The hydration number for calcium in solution with small anions showed a dependence on salinity, ranging between 6 and 7.5 water molecules in the first hydration shell. For large counterions, like bromide and iodide, the hydration number remained almost constant between 7.5 and 8. This large hydration number is in very good agreement with experimental work that determined the number of water molecules in the first hydration shell to be

8.[40] On average, a water molecule remained within the first hydration shell around the cation for 131 ps. To leave the shell, an energy barrier of roughly $6\,k_\mathrm{B}T$ had to be overcome, which leads to a minimum rate coefficient of $k_\mathrm{T} = 0.059\,\mathrm{ps}^{-1}$. For the present model, the transmission coefficient was determined to be $\kappa \approx 0.13$.

Strontium: The RDF of water around strontium exhibits the first maximum at a distance of 2.5 Å from the ion, which is close to the experimentally observed value of 2.6 Å[40,48] and is in excellent agreement with ab initio calculations performed without counterions.[49] The first minimum was observed at 3.1 Å. The locations of the second extrema of the RDF were determined to be 4.7 and 5.4 Å, respectively. The peak is slightly smaller than observed by ab initio calculations.[49] The hydration number in the first shell of Sr^{2+} was calculated to be $n_{i-\mathrm{O}} \approx 8$, which is in excellent agreement with the experimental data at high salinity, being 7.9 to 8.[41] The hydration number showed no dependence on counterion type and salinity. On average, a water molecule remained in the first hydration shell of strontium for 105 ps. For an exchange of a water molecule in the first shell, an energy barrier of roughly $6\,k_\mathrm{B}T$ had to be overcome. The maximum rate of water molecule replacements in the first shell was determined to be $0.015\,\mathrm{ps}^{-1}$, resulting in a transmission coefficient of $\kappa = 0.63$.

Barium: For barium, the first maximum of the RDF was found at 2.6 Å and the first minimum at 3.2 Å. These values differ from experimental data by 0.2 to 0.33 Å.[40,50] Ab initio calculations performed without counterions suggest a maximum of 2.8 Å.[51] The following extrema in the RDF were determined to be at 4.8 and 5.7 Å. The hydration number was 8, independent on counterion type and salinity. The residence time of water molecules within the first shell was 40 ps. Removing a water molecule from the first shell is associated with an energy barrier of roughly $5.5\,k_\mathrm{B}T$ and the rate constant was $0.026\,\mathrm{ps}^{-1}$, resulting in a transmission coefficient close to unity.

Self-diffusion coefficient

For all alkaline-earth cations in aqueous chloride solutions, the self-diffusion coefficient D_i was determined at $T = 298.15\,\mathrm{K}$ and $p = 1\,\mathrm{bar}$. Here, the different electrolyte solutions contain a constant

number of cations ($x_{MgCl2} = 0.03$ g/g, $x_{CaCl2} = 0.04$ g/g, $x_{SrCl2} = 0.05$ g/g and $x_{BaCl2} = 0.07$ g/g). The self-diffusivity is a measure for the ion mobility in solution and is therefore highly influenced by the ion-solvent interactions and hence, the water force field, which was SPC/E[24] in this study. Due to the strong ion-solvent attraction, ions do not diffuse in solution as single particles, but together with the water molecules in their first shell. The ion-water complex can be described by a sphere with an effective radius that increases with stronger attractive forces between ion and water molecules. Within the complex, ion motion is short-ranged and fast, but does not contribute significantly to the ion self-diffusion coefficient.[31] A typical velocity autocorrelation function observed for an aqueous CaCl$_2$ solution is shown in Figure 3. Here, the motion of the water molecules in the first hydration shell with respect to the bulk water and the motion of the ion relative to its hydration shell contribute to the total motion of the Ca^{2+} cation. According to Impey et al.,[31] the oscillations of the velocity autocorrelation function indicate a faster motion of the ion within its first hydration shell.

Overall, the self-diffusion coefficient of the cations agrees well with experimental data,[52] cf. Figure 4 and Table 3. The diffusion coefficient shows only little dependence on the cation size, which is in agreement with experimental data. This independence is due to the hydration dynamics around the ions. Smaller cations are supposed to diffuse faster in solution, however, the attractive forces that these ions exert on the water molecules are larger. Thus, solvent molecules are more attached to the ion, forming a stable ion-water complex with a large effective radius. For large cations, the electrostatic attraction between ion and water is less dominant. However, because of their large diameter, the effective radius of the hydration sphere is very similar to the one of small cations so that D_i does not significantly depend on the alkaline-earth cation species in aqueous solutions.

Electric conductivity

The electric conductivity σ was determined for aqueous MgCl$_2$ and BaCl$_2$ solutions for varying salinity at ambient conditions to study the cation size dependence of σ. These two salts were chosen, because sufficient experimental data is available. The agreement with experimental data[30,53]

is excellent, cf. Figure 5. For salinities of up to 0.09 g/g for $MgCl_2$ and 0.18 g/g for $BaCl_2$, the deviations are below 13 %. The calculation of σ by molecular simulation gives further insight into the dynamics of the ions in solution. By separating the electric conductivity into the two terms according Eq. (13), the contribution of the correlated ion motions was determined. This analysis was performed for aqueous $MgCl_2$ and $BaCl_2$ solutions containing a constant number of cations ($x_{MgCl2} = 0.09$ g/g and $x_{BaCl2} = 0.18$ g/g). The results of this analysis are discussed below and are shown in Figure 6 and Figure 7.

Magnesium: For very short times ($t < 0.01$ ps), the crosscorrelation $\Delta(t)$ is positive. This is due to the random motions of the cation within its first hydration shell, which are dominated by the interactions of the cation with its nearest water molecules only. These motions are superimposed by the correlated motions of the cation with the anion due to their electrostatic attraction. For the chloride anion, the correlated motions are fully developed and show a characteristic behavior that is dominated by the electrostatic repulsion. Hence, $\Delta(t)$ is positive. For longer times, the cage motions of Mg^{2+} are superimposed by the characteristic long time motion of the ion grouped with its hydration shell. $\Delta(t)$ is negative in this case, indicating the expected correlated motions of anion and cation. The rapid motions of Mg^{2+} within its hydration shell lead to oscillations of $\Delta(t)$ over time that are depicted in Figure 6 and that can also be seen for $Z(t)$. Within 0.8 ps, Mg^{2+} shows eight changes in direction due to the interactions with its hydration shell.

Barium: In aqueous $BaCl_2$ solutions, the oscillations of $Z(t)$ and $\Delta(t)$ are less pronounced, cf. Figure 7, since the motions of larger cations within their first hydration shell are less rapid. Looking at the motions of the anions and the cations in detail, correlated motions of oppositely charged ions ($\Delta(t) < 0$) were observed only for short times ($t < 0.44$ ps). At longer times, $\Delta(t)$ is positive, which indicates correlated motions of ions of the same charge. The strong attractive forces between oppositely charged ions lead to a frequent exchange of the interaction partners in terms of correlated motions. Hence, $\Delta(t)$ is dominated for longer times by correlated motions of ions of the same charge, which is attributed to electrostatic repulsion.

Comparing the behavior of the ions, correlated motions of oppositely charged ions ($\Delta(t) < 0$)

were observed in both of the studied aqueous alkaline-earth chloride solutions. For MgCl$_2$, the absolute value of $\Delta(t)$ is significantly smaller than in case of BaCl$_2$. Correlated motions of ions highly depend on the ability of the anions to replace water molecules in the hydration shell of the alkaline-earth cations. For both cations, no chloride ions were observed in the first hydration shell. In this case, the correlated motions of the ions were caused by interactions between ions that are separated by one or more water molecules. For Mg^{2+}, the strong attraction between cation and water molecules in the second hydration shell inhibits a continuous exchange of water molecules. Hence, the chloride anion is not able to replace water molecules in the second hydration shell and therefore, correlated motions are unlikely to occur. In contrast, there is more exchange of water molecules around the Ba^{2+} cation and thus correlated motions are more pronounced.

Enthalpy of hydration

The enthalpy of hydration of alkaline-earth salts in aqueous solutions was determined. The results were obtained from molecular simulation at low salinity (10 cations, 20 anions and 970 water molecules) at $T = 298.15$ K and $p = 1$ bar and are summarized in Table 2. The agreement between data from simulation and experiment [38] is good for all salts, except for BeCl$_2$, where also some deviations for the structural properties were found. For the remaining salts, the deviations are below 10%, which is roughly the accuracy of the experimental data.[38] The deviations decrease with increasing ion size, which is not surprising, because for these solutions also a better agreement with respect to the reduced solution density and other thermodynamic and structural data was achieved. The ion force fields also correctly predict the qualitative trend that the enthalpy of hydration decreases with increasing ion size.

5. Conclusions

Molecular models for the alkaline-earth ions based on the LJ approach with a superimposed point charge were developed. The force fields were parameterized using experimental data on the re-

duced liquid solution density of five electrolyte solutions, mainly containing the bromide anion at low salinity. These density data were reproduced exactly.

The present force fields can be applied in any mutual combination for the alkaline-earth halide salts. This was shown by predictive calculations using the reduced liquid solution density as a reference. The present simulations showed an excellent agreement with experimental data for all studied aqueous electrolyte solutions at low salinity. At high salinity, the present force fields were also found to be very accurate for alkaline-earth bromides and iodides, while for alkaline-earth chloride solutions the deviations from experimental density data were more significant.

The force fields were also investigated with respect to structural and dynamic properties. For the RDF and the hydration number, a very good agreement was found for all electrolyte solutions, except for $BeCl_2$. In this case, the attractive forces between the solvent and the ion model seem to be too strong and hence the ordering around the cation was overpredicted. For all cations, the RDF clearly indicated two hydration shells that are strongly developed. In the first shell, a very stable structure around the cations was observed. The oxygen atoms of the surrounding water molecules are oriented towards the cation and their rotational motions are hindered by the strong electrostatic attraction with the cation. The second shell is located 4 to 5 Å from the cation. There, the influence of the cation onto the solution is weaker, however, it is still significant.

Calculations of the potential of mean force suggest that the exchange of water molecules from the first to the second shell is hindered by a large energy barrier. This barrier decreases with increasing cation size and ranges between $\approx 6\,k_{\mathrm{B}}T$ and $> 8\,k_{\mathrm{B}}T$. The height of the energy barrier correlates with the hydration dynamics, i.e. the residence time of water molecules in the first hydration shell increases with a higher energy barrier, while the rate coefficient decreases.

The cation mobility in solution was studied by means of the self-diffusion coefficient. For all alkaline-earth cations in aqueous halide solutions, the self-diffusion coefficient is in good agreement with the experimental data. The deviations from experimental data are less than 15%. The self-diffusion coefficient of the cations showed hardly any dependence on the ion size, which is in agreement with experimental observations.

The electric conductivity was determined for aqueous $MgCl_2$ and $BaCl_2$ solutions over a wide range of salinity. The agreement with experimental data is excellent. For both solutions, the influence of the cation size on the auto- and the crosscorrelation contribution to the electric conductivity was investigated. This analysis showed the ion size dependence of the electric conductivity. For small cations, the ion motions tend to be highly correlated with the counterion. This behavior, however, is superimposed by short range ion motions within their first hydration shell, especially at short times. For large cations, the correlated motions are similar for short times, but are different for long times. This is attributed to the short lifetime of correlated motions of oppositely charged ions and the long term electrostatic repulsion of evenly charged ions.

The solution was further studied with respect to the enthalpy of hydration. This quantity was predicted for all alkaline-earth halide solutions and also shows a very good agreement with experimental data, being mostly within the combined error bars.

Acknowledgments

Appendix

The present simulation study was performed with an extended version of *ms*2.[54] For the static properties, the classical Monte-Carlo (MC) method was employed. In MC, all simulations were performed in the isothermal-isobaric (NpT) ensemble at 293.15 K and 1 bar. Electrostatic long range contributions were considered by Ewald summation[55] with a real space convergence param-

eter $\kappa = 5.6$. The ions and the solvent molecules were initially placed onto a face-centered cubic lattice in random order. A physically reasonable configuration was obtained by $5,000$ equilibration loops in the canonical ensemble, followed by $80,000$ relaxation loops in the NpT ensemble. Thermodynamic averages were obtained over $500,000$ loops. Each loop consisted of $N_{\mathrm{NDF}}/3$ steps, where N_{NDF} indicates the total number of mechanical degrees of freedom of the system. Configurations of the system were saved every 500 loops, which were used for the calculation of the RDF via post-processing. For the calculation of dynamic properties of the aqueous electrolyte solutions, MD simulations were performed. The self-diffusion coefficient of the ions and the electric conductivity of the solution were calculated with the Green-Kubo formalism.[34,35] First, the density of the electrolyte solution was determined by a NpT simulation at the desired temperature and pressure. Subsequently, the self-diffusion coefficient was sampled in the canonic (NVT) ensemble at the temperature and the density resulting from the first step. The sampling length of the velocity and the electric current correlation functions was set to 11 ps and the separation between the origin of two autocorrelation functions was 0.06 ps. Within this time span, all autocorrelation functions decayed to less than 1/e of their normalized value.

For all simulations in the NpT ensemble, a physically reasonable configuration was attained by $10,000$ steps in the NVT ensemble and $100,000$ steps in the NpT ensemble, followed by a production run over $500,000$ time steps. For simulations in the NVT ensemble, the equilibration was performed over $100,000$ steps, followed by a production run of $1,800,000$ and $2,400,000$ time steps for the determination of the self-diffusion coefficient and the electric conductivity, respectively. Newton's equations of motion were solved with a Gear predictor-corrector scheme of fifth order with a time step of 1.2 ps. The MD unit cell with periodic boundary conditions contained 4500 molecules. For the calculation of the self-diffusion coefficient, the simulation volume contained 4419 water molecules, 27 alkaline-earth ions and 54 chloride ions. The electric conductivity was determined for different salinities. Hence, the number of alkaline-earth ions in the simulation volume varied from 4 to 81. The electrostatic long range contributions were considered in the same way as in case of the MC simulations.

List of Figures

Figure 1: Reduced liquid solution density $\widetilde{\rho}$ of aqueous solutions of different alkaline-earth halide salts over salinity at $T = 293.15$ K and $p = 1$ bar. Present simulation data (symbols) are compared to correlations of experimental data[39] (lines).
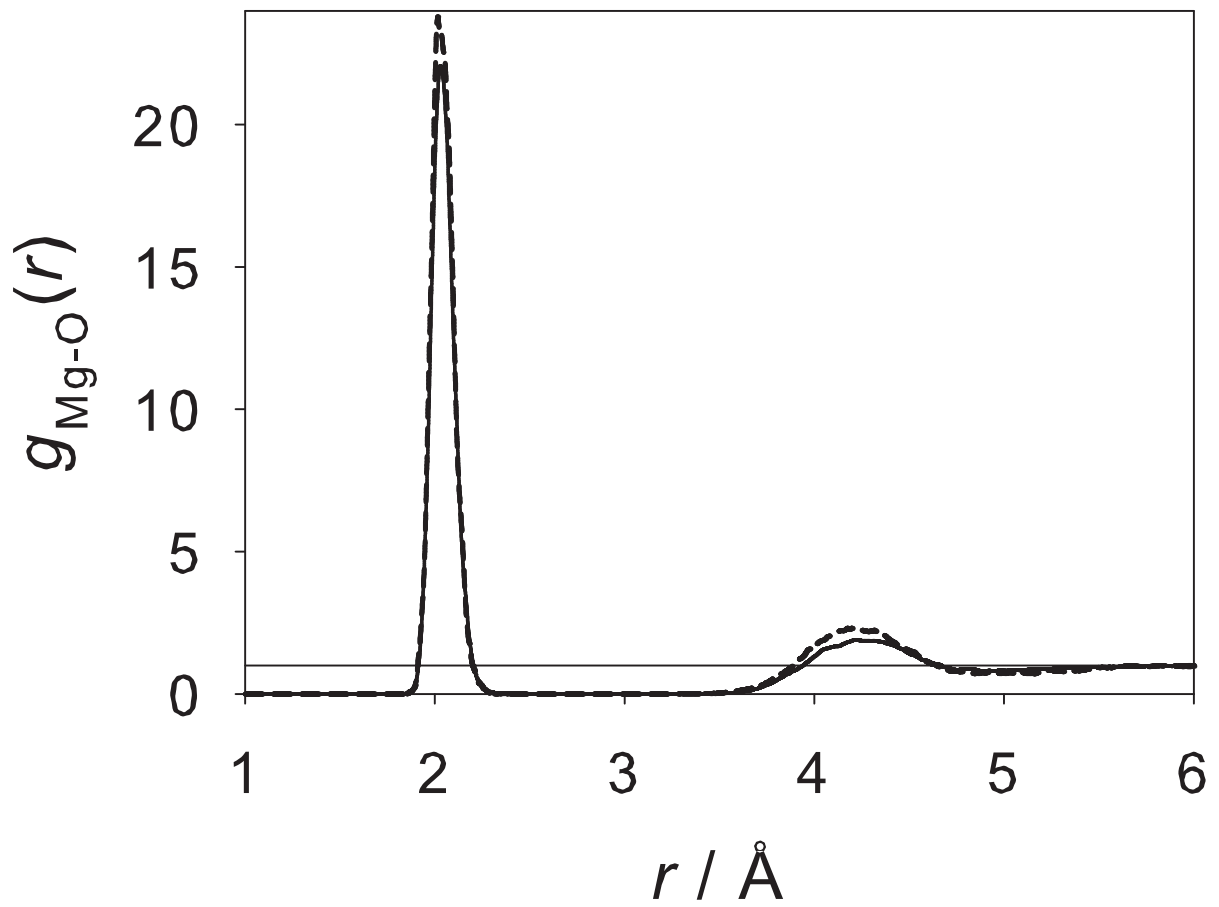
Figure 2: Radial distribution function around the magnesium cation Mg^{2+} in an aqueous $MgCl_2$ solution at $T = 293.15$ K and $p = 1$ bar for two salinities. Dashed line: $x_{MgCl2} = 0.06$ g/g, solid line: $x_{MgCl2} = 0.17$ g/g.
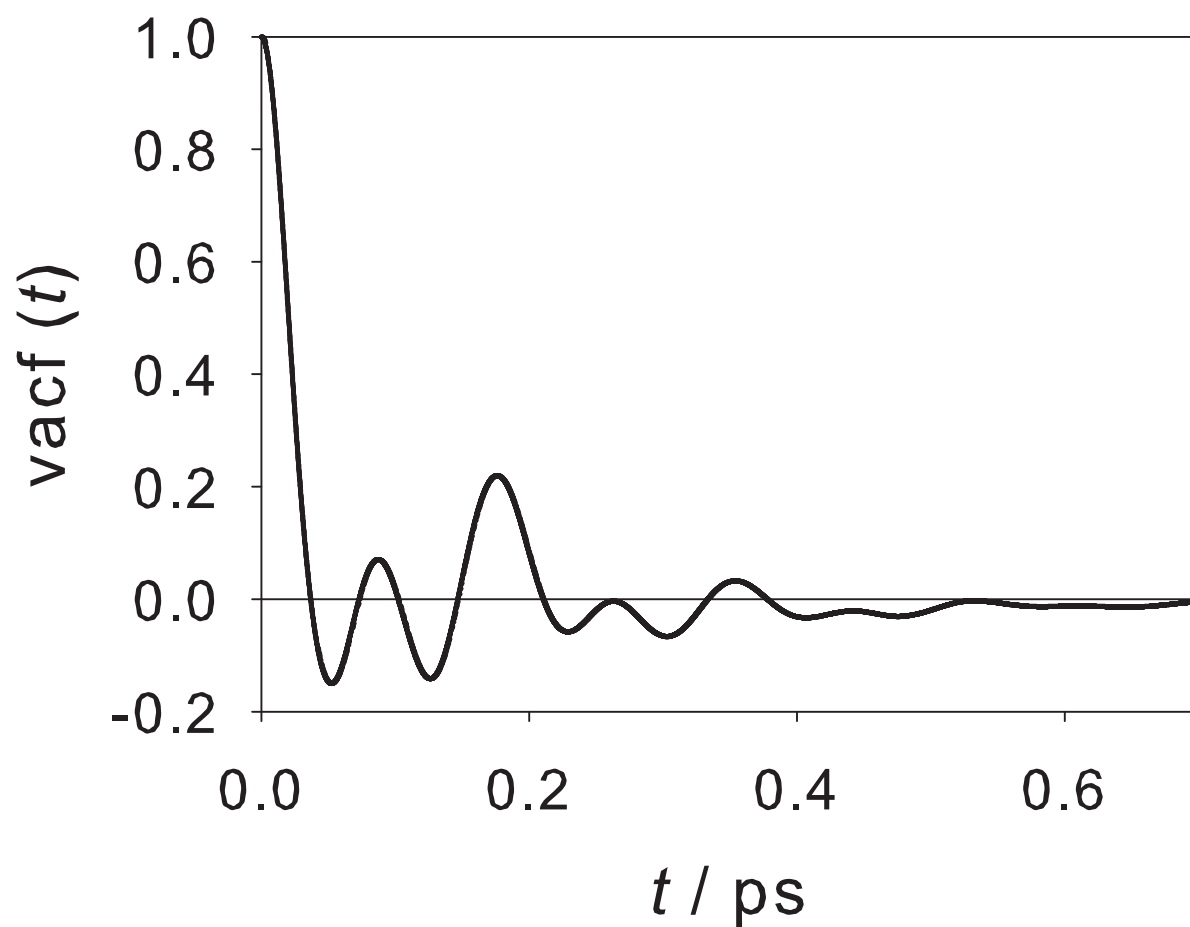
Figure 3: Normalized velocity autocorrelation function (vacf) of calcium Ca^{2+} in an aqueous $CaCl_2$ solution ($x_{CaCl2} = 0.04$ g/g) at $T = 298.15$ K and $p = 1$ bar.
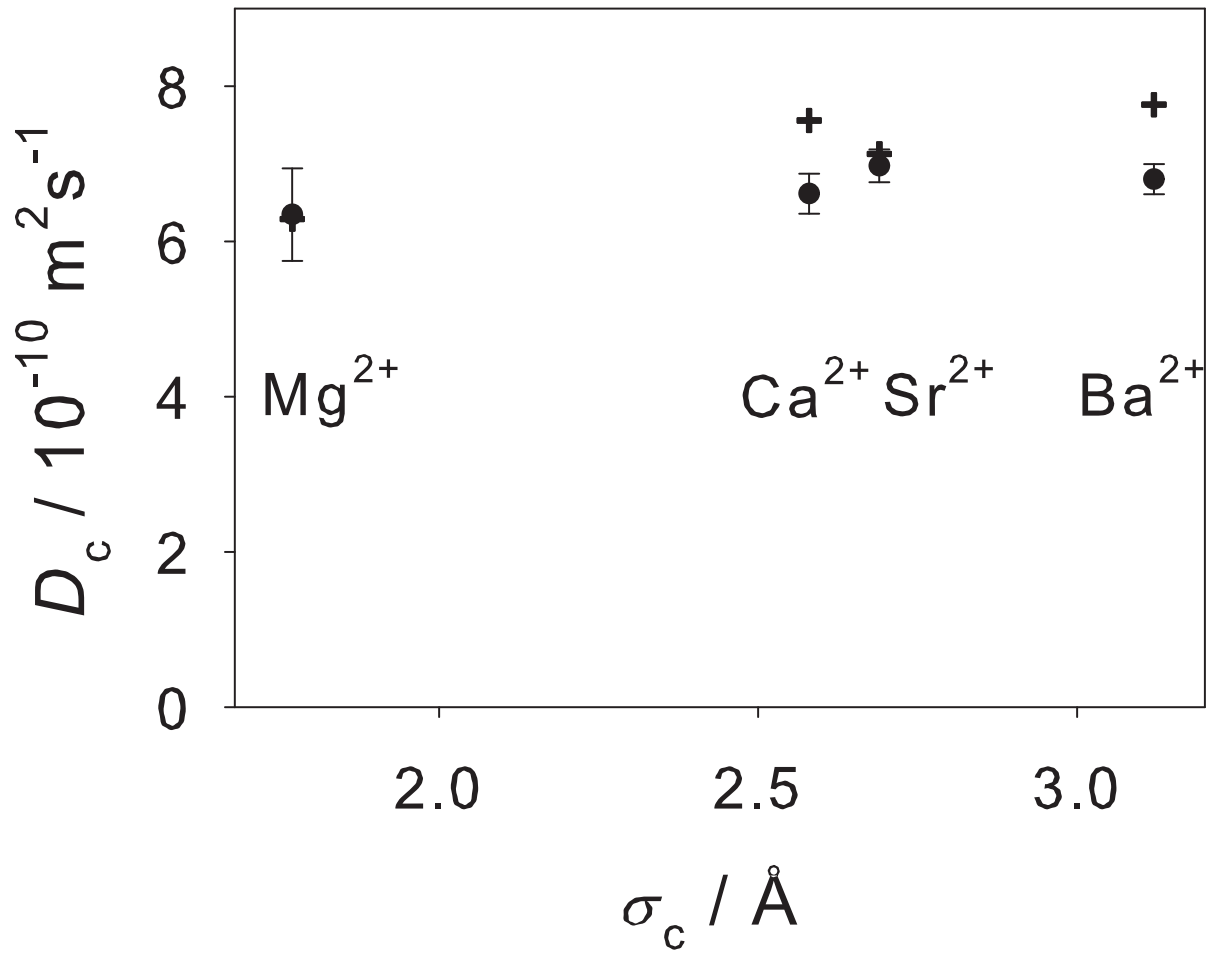
Figure 4: Self-diffusion coefficient of alkaline-earth cations in aqueous solutions containing a constant number of cations ($x_{MgCl2} = 0.03$ g/g, $x_{CaCl2} = 0.04$ g/g, $x_{SrCl2} = 0.05$ g/g and $x_{BaCl2} = 0.07$ g/g) at $T = 298.15$ K and $p = 1$ bar: present simulation results (●) are compared to experimental data (+).[52]
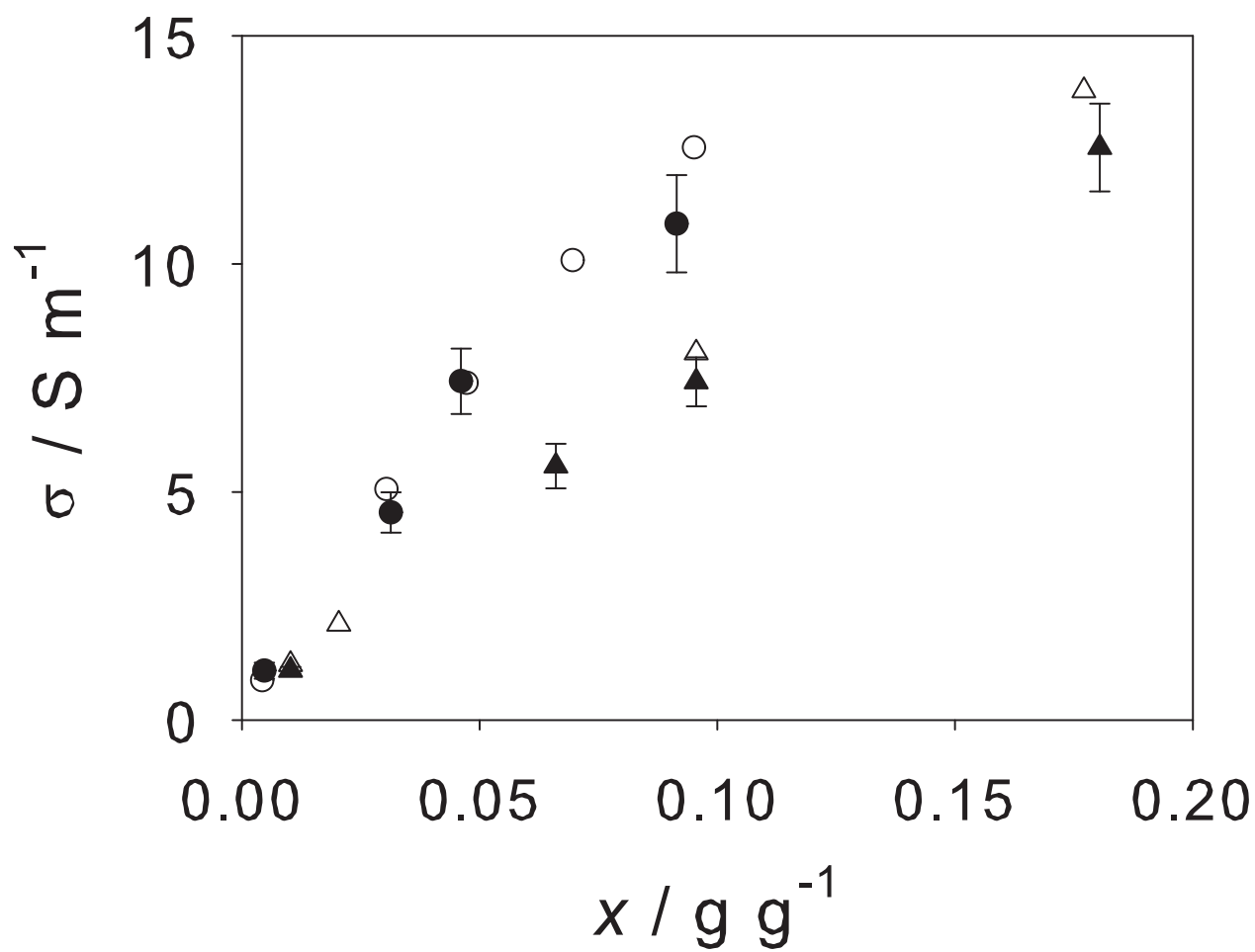
Figure 5: Electric conductivity σ as a function of salinity in aqueous $MgCl_2$ ($\bullet$) and $BaCl_2$ ($\blacktriangle$) solutions at $T = 298.15$ K and $p = 1$ bar. Simulation results (full symbols) are compared to experimental data (empty symbols).[30,53]
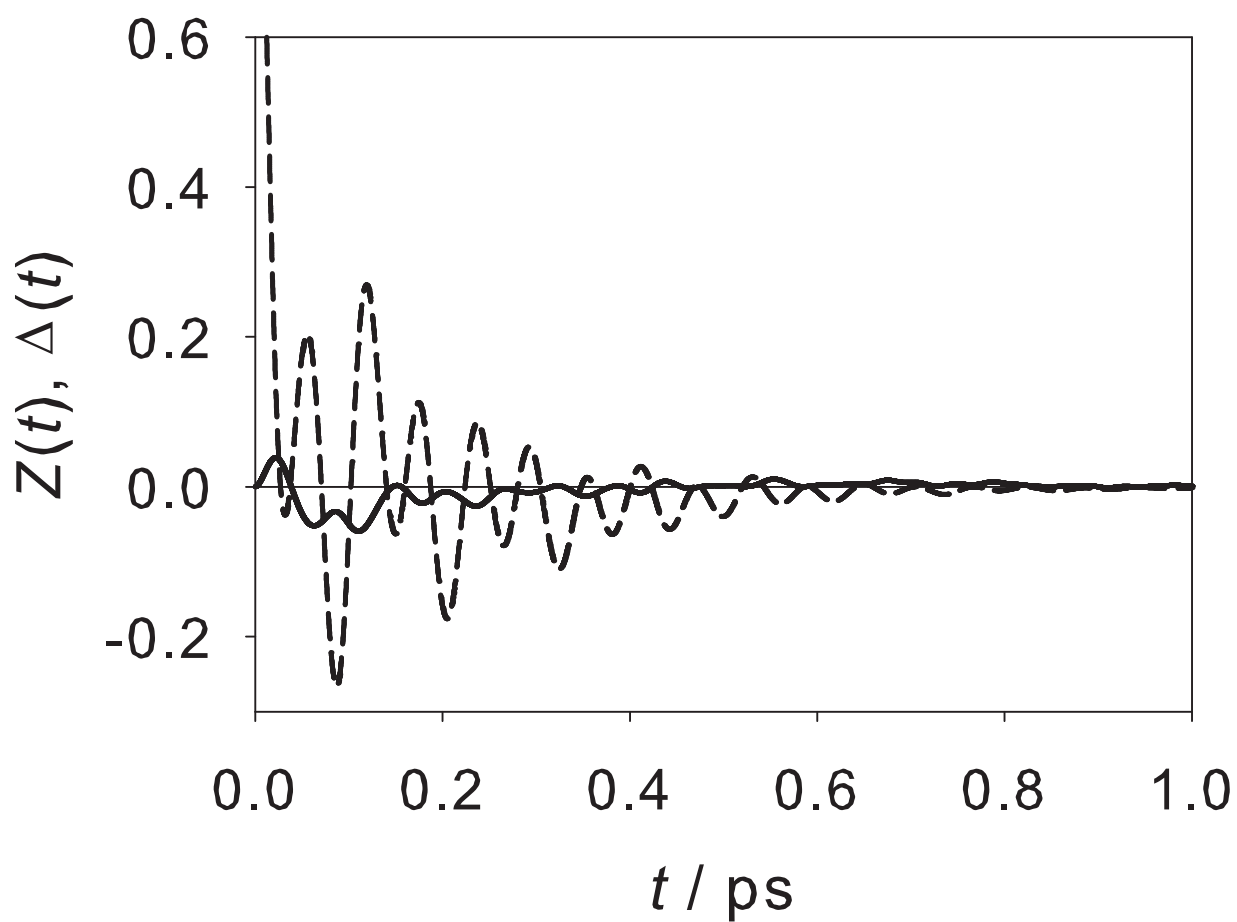
Figure 6: Electric current time autocorrelation function of $MgCl_2$ in aqueous solution ($x_{MgCl2} = 0.09$ g/g) at $T = 298.15$ K and $p = 1$ bar separated into its contributions: velocity autocorrelation function $Z(t)$ (dashed line), velocity crosscorrelation function $\Delta(t)$ (solid line).
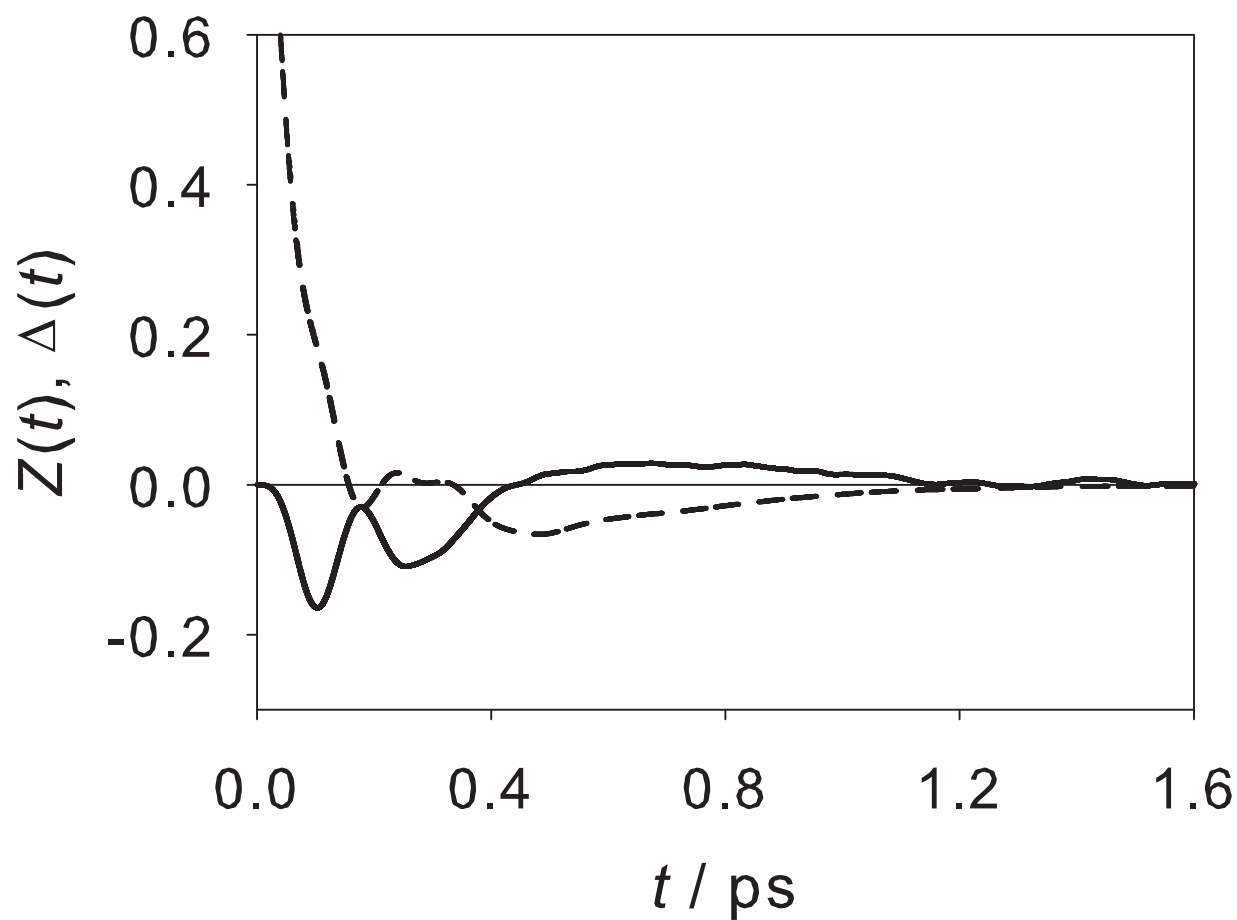
Figure 7: Electric current time autocorrelation function for $BaCl_2$ in aqueous solution ($x_{BaCl_2} = 0.18$ g/g) at $T = 298.15$ K and $p = 1$ bar separated into its contributions: velocity autocorrelation function $Z(t)$ (dashed line), velocity crosscorrelation function $\Delta(t)$ (solid line). Note that the vertical scale is the same as in Figure 6

.

Table 1: Lennard-Jones size parameter σ for alkaline-earth cations determined in the present work and for halide anions taken from preceding work[23] that were used here. The LJ energy parameter was $\varepsilon/k_B = 200$ **K for all ions.**

Ion	σ / Å	q / e
Be^{2+}	1.69	+2
Mg^{2+}	1.77	+2
Ca^{2+}	2.58	+2
Sr^{2+}	2.69	+2
Ba^{2+}	3.12	+2
F^-	3.66	−1
Cl^-	4.41	−1
Br^-	4.54	−1
I^-	4.78	−1

Table 2: Properties of aqueous electrolyte solutions at $T = 293.15$ K and $p = 1$ bar determined by present molecular simulations: distances of the first $r_{\mathrm{max},1}$ and second maximum $r_{\mathrm{max},2}$ as well as first $r_{\mathrm{min},1}$ and second minimum $r_{\mathrm{min},2}$ of the ion-water RDF. The hydration numbers $n_{i-\mathrm{O}}$ are given for varying salinity in terms of the molality $x^{(\mathrm{M})}$. The enthalpy of hydration $\Delta h_{\mathrm{hyd}}^{\mathrm{Exp.}}$ is given at infinite dilution and compared to experimental data.[38] The number in parenthesis indicates the statistical uncertainty in the last digit. The experimental mean distances between the ions and the oxygen atom of water in the first hydration shell are: $r_{\mathrm{max},1}^{\mathrm{Be}^{2+}} = 1.75$ Å, $r_{\mathrm{max},1}^{\mathrm{Mg}^{2+}} = 2.1$ Å, $r_{\mathrm{max},1}^{\mathrm{Ca}^{2+}} = 2.4$ Å, $r_{\mathrm{max},1}^{\mathrm{Sr}^{2+}} = 2.6$ Å and $r_{\mathrm{max},1}^{\mathrm{Ba}^{2+}} = 2.9$ Å.[40]

Salt	$r_{\mathrm{max},1}$ Å	$r_{\mathrm{min},1}$ Å	$r_{\mathrm{max},2}$ Å	$r_{\mathrm{min},2}$ Å	$n_{i-\mathrm{O}}$ (1 M) -	$n_{i-\mathrm{O}}$ (3 M) -	$-\Delta h_{\mathrm{hyd}}$ kJ mol^{-1}	$-\Delta h_{\mathrm{hyd}}^{\mathrm{Exp.}}$ kJ mol^{-1}
BeCl$_2$	2.0	2.3	4.2	4.9	6.5	5.4	2461(1)	3256
MgCl$_2$	2.0	2.3	4.2	4.9	5.9	5.3	2462(1)	2683
MgBr$_2$	2.0	2.3	4.2	4.9	5.8	5.4	2430(1)	2615
MgI$_2$	2.0	2.3	4.2	4.9	5.9	5.3	2378(1)	2531
CaCl$_2$	2.4	3.0	4.6	5.4	7.8	6.9	2147(1)	2339
CaBr$_2$	2.4	3.0	4.6	5.4	7.9	7.4	2117(1)	2271
CaI$_2$	2.4	3.0	4.6	5.4	7.8	7.5	2066(1)	2187
SrCl$_2$	2.5	3.1	4.7	5.5	7.9	7.6	2111(1)	2205
SrBr$_2$	2.5	3.1	4.7	5.5	8.0	7.3	2084(1)	2137
SrI$_2$	2.5	3.1	4.7	5.5	8.0	7.9	2031(1)	2053
BaCl$_2$	2.6	3.2	4.8	5.7	8.4	7.8	1972(1)	2067
BaBr$_2$	2.6	3.2	4.8	5.7	8.3	7.7	1940(1)	1999
BaI$_2$	2.6	3.2	4.8	5.7	8.4	8.2	1891(1)	1915

Table 3: Properties of aqueous electrolyte solutions at $T = 298.15$ K and $p = 1$ bar determined by present molecular simulations: rate coefficient k, maximum rate coefficient determined by transition state theory k^{T}, transmission coefficient κ and self-diffusion coefficient D_i. The number in parenthesis indicates the statistical uncertainty in the last digit.

Ion i	k / ps^{-1}	k^{T} / ps^{-1}	κ	D_i / 10^{-10} m^2 s^{-1}
Be^{2+}	<0.0003	0.000	-	-
Mg^{2+}	<0.0003	0.000	-	6.5(6)
Ca^{2+}	0.0076	0.059	0.13	7.7(3)
Sr^{2+}	0.0095	0.015	0.63	7.2(2)
Ba^{2+}	0.0249	0.026	0.95	7.9(2)

References

(1) Debye, P.; Huckel, E. *Physikalische Zeitschrift* **1923**, *24*, 185–206.

(2) Debye, P.; Huckel, E. *Physikalische Zeitschrift* **1923**, *24*, 185–206.

(3) Chen, C. C.; Britt, H. I.; Boston, J. F.; Evans, L. B. *AIChE Journal* **1982**, *28*, 588–596.

(4) Chen, C. C.; Evans, L. B. *AIChE Journal* **1986**, *32*, 444–454.

(5) Pitzer, K. S. *Journal of Physical Chemistry* **1973**, *77*, 268–277.

(6) Pitzer, K. S.; Mayorga, G. *Journal of Physical Chemistry* **1973**, *77*, 2300–2308.

(7) Pitzer, K. S.; Mayorga, G. *Journal of Solution Chemistry* **1974**, *3*, 539–546.

(8) Sambriski, E. J.; Schwartz, D. C.; de Pablo, J. J. *Proceedings of the National Academy of Sciences of the United States of America* **2009**, *106*, 18125–18130.

(9) Shi, W.; Inamdar, M. V.; Sastry, A. M.; Lastoskie, C. M. *Journal of Physical Chemistry C* **2007**, *111*, 15642–15652.

(10) Dietz, W.; Riede, W. O.; Heinzinger, K. *Zeitschrift Naturforschung Section A* **1982**, *37*, 1038–1048.

(11) Probst, M. M.; Radnai, T.; Heinzinger, K.; Bopp, P.; Rode, B. M. *Journal of Physical Chemistry* **1985**, *89*, 753–759.

(12) Guardia, E.; Robinson, A.; Padro, J. A. *The Journal of Chemical Physics* **1993**, *99*, 4229–4230.

(13) Koneshan, S.; Rasaiah, J. C.; Lynden-Bell, R. M.; Lee, S. H. *Journal of Physical Chemistry B* **1998**, *102*, 4193–4204.

(14) Aqvist, J. *Journal of Physical Chemistry* **1990**, *94*, 8021–8024.

(15) Cornell, W. D.; Cieplak, P.; Bayly, C. I.; Gould, I. R.; Merz, K. M.; Ferguson, D. M.; Spellmeyer, D. C.; Fox, T.; Caldwell, J. W.; Kollman, P. A. *Journal of the American Chemical Society* **1995**, *117*, 5179–5197.

(16) Ponder, J. W.; Case, D. A. *Protein Simulations* **2003**, *66*, 27–85.

(17) Spangberg, D.; Hermansson, K. *The Journal of Chemical Physics* **2004**, *120*, 4829–4843.

(18) Jiao, D.; King, C.; Grossfield, A.; Darden, T. A.; Ren, P. Y. *Journal of Physical Chemistry B* **2006**, *110*, 18553–18559.

(19) Megyes, T.; Bako, I.; Balint, S.; Grosz, T.; Radnai, T. *Journal of Molecular Liquids* **2006**, *129*, 63–74.

(20) Gavryushov, S.; Linse, P. *Journal of Physical Chemistry B* **2006**, *110*, 10878–10887.

(21) Towhee, http://www.towhee.sourceforge.org. 2008.

(22) Hess, B.; Kutzner, C.; van der Spoel, D.; Lindahl, E. *Journal of Chemical Theory and Computation* **2008**, *4*, 435–447.

(23) Deublein, S.; Vrabec, J.; Hasse, H. *The Journal of Chemical Physics* **2012**, *accepted*.

(24) Berendsen, H. J. C.; Grigera, J. R.; Straatsma, T. P. *Journal of Physical Chemistry* **1987**, *91*, 6269–6271.

(25) Lorentz, H. *Annalen der Physik* **1881**, *248*, 127–136.

(26) Berthelot, D. *Comptes Rendues de l'Academie des Sciences* **1898**, *126*, 1703–1706.

(27) Christen, M.; Hunenberger, P. H.; Bakowies, D.; Baron, R.; Burgi, R.; Geerke, D. P.; Heinz, T. N.; Kastenholz, M. A.; Krautler, V.; Oostenbrink, C.; Peter, C.; Trzesniak, D.; Van Gunsteren, W. F. *Journal of Computational Chemistry* **2005**, *26*, 1719–1751.

(28) Deublein, S.; Reiser, S.; Vrabec, J.; Hasse, H. *in preparation* **2012**,

(29) Allen, M.; Tildesley, D. *Computer Simulation of Liquids*; Clarendon Press: Oxford, 1987.

(30) Robinson, R. A.; Stokes, R. H. *Electrolyte Solutions*, 2nd ed.; Butterworth: London, 1955.

(31) Impey, R. W.; Madden, P. A.; McDonald, I. R. *Journal of Physical Chemistry* **1983**, *87*, 5071–5083.

(32) Ciccotti, G.; Ferrario, M.; Hynes, J. T.; Kapral, R. *The Journal of Chemical Physics* **1990**, *93*, 7137–7147.

(33) Rey, R.; Hynes, J. T. *Journal of Physical Chemistry* **1996**, *100*, 5611–5615.

(34) Gubbins, K. *Statistical Mechanics Vol. 1*; The Chemical Society Burlington House: London, 1972.

(35) Hansen, J. P.; McDonald, I. *Theory of Simple Liquids*; Academic Press: Amsterdam, 1986.

(36) Del Popolo, M. G.; Voth, G. A. *Journal of Physical Chemistry B* **2004**, *108*, 1744–1752.

(37) Chandrasekhar, J.; Jorgensen, W. L. *The Journal of Chemical Physics* **1982**, *77*, 5080–5089.

(38) Riedel, E. *Allgemeine und Anorganische Chemie*, 10th ed.; Gruyter: Berlin, 2010.

(39) Weast, R. *Handbook of Chemistry and Physics*, 68th ed.; CRC Press: Boca Raton, 1987.

(40) Marcus, Y. *Chemical Reviews* **1988**, *88*, 1475–1498.

(41) Ohtaki, H.; Radnai, T. *Chemical Reviews* **1993**, *93*, 1157–1204.

(42) Azam, S. S.; Hofer, T. S.; Bhattacharjee, A.; Lim, L. H. V.; Pribil, A. B.; Randolf, B. R.; Rode, B. M. *Journal of Physical Chemistry B* **2009**, *113*, 9289–9295.

(43) Masia, M.; Rey, R. *The Journal of Chemical Physics* **2005**, *122*, 094502.

(44) Caminiti, R.; Licheri, G.; Piccaluga, G.; Pinna, G. *Journal of Applied Crystallography* **1979**, *12*, 34–38.

(45) Tongraar, A.; Rode, B. M. *Chemical Physics Letters* **2005**, *409*, 304–309.

(46) Smirnov, P. R.; Trostin, V. N. *Russian Journal of General Chemistry* **2008**, *78*, 1643–1649.

(47) Schwenk, C. F.; Rode, B. M. *Pure and Applied Chemistry* **2004**, *76*, 37–47.

(48) Caminiti, R.; Musinu, A.; Paschina, G.; Pinna, G. *Journal of Applied Crystallography* **1982**, *15*, 482–487.

(49) Hofer, T. S.; Randolf, B. R.; Rode, B. M. *Journal of Physical Chemistry B* **2006**, *110*, 20409–20417.

(50) Persson, I.; Sandstroem, M.; Yokoyama, H.; Chaudhry, M. *Zeitschrift Naturforschung Section A* **1995**, *50*, 21–37.

(51) Hofer, T. S.; Rode, B. M.; Randolf, B. R. *Chemical Physics* **2005**, *312*, 81–88.

(52) Mills, R.; Lobo, V. *Self-diffusion in electrolyte solutions*; Elsevier: New York, 1989.

(53) Than, A.; Amis, E. *Journal of Inorganic and Nulcear Chemistry* **1969**, *31*, 1685–1695.

(54) Deublein, S.; Eckl, B.; Stoll, J.; Lishchuk, S.; Guevara-Carrion, G.; Glass, C.; Merker, T.; Bernreuther, M.; Hasse, H.; Vrabec, J. *Computer Physics Communications* **2011**, *182*, 2350–2367.

(55) Ewald, P. P. *Annalen der Physik* **1921**, *64*, 253–287.